Individual Muscle Force Estimation in the Human Forearm using Multi-Muscle MR Elastography (MM-MRE)

Daniel R. Smith[*], Cody A. Helm[*], Andrea Zonnino, Matthew D.J. McGarry,
Curtis L. Johnson[*], and Fabrizio Sergi[*]

Abstract— Objective: **To establish the sensitivity of magnetic resonance elastography (MRE) to active muscle contraction in multiple muscles of the forearm.** *Methods:* **We combined MRE of forearm muscles with an MRI-compatible device, the MREbot, to simultaneously measure the mechanical properties of tissues in the forearm and the torque applied by the wrist joint during isometric tasks. We measured shear wave speed of thirteen forearm muscles via MRE in a series of contractile states and wrist postures and fit these outputs to a force estimation algorithm based on a musculoskeletal model.** *Results:* **Shear wave speed changed significantly upon several factors, including whether the muscle was recruited as an agonist or antagonist (p=0.0019), torque amplitude (p=<0.0001), and wrist posture (p=0.0002). Shear wave speed increased significantly during both agonist (p=<0.0001) and antagonist (p=0.0448) contraction. Additionally, there was a greater increase in shear wave speed at greater levels of loading. The variations due to these factors indicate the sensitivity to functional loading of muscle. Under the assumption of a quadratic relationship between shear wave speed and muscle force, MRE measurements accounted for an average of 70% of the variance in the measured joint torque.** *Conclusion:* **This study shows the ability of MM-MRE to capture variations in individual muscle shear wave speed due to muscle activation and presents a method to estimate individual muscle force through MM-MRE derived measurements of shear wave speed.** *Significance:* **MM-MRE could be used to establish normal and abnormal muscle co-contraction patterns in muscles of the forearm controlling hand and wrist function.**

Index Terms—**Force estimation, Magnetic Resonance Elastography, Muscle Contraction.**

I. INTRODUCTION

OBJECT manipulation allows for interactions between an individual and their environment, though this is one of the most complex motor functions that requires the proper and coordinated activation of skeletal muscles with high accuracy to perform tasks [1]. The neuromuscular system exerts control over the muscles to manipulate objects, which can be analyzed through either the inputs or outputs of neuromuscular activation to understand contributions to successful task completion [2]. Measuring the neuromuscular input signal to muscles can be used to understand the control of motion. However, current non-invasive methods used for this purpose (such as surface electromyography, sEMG) cannot differentiate between the contributions of the signals sent to the individual muscles when the muscles are not superficial nor sufficiently spaced apart. Alternatively, the outputs of the neuromuscular system – i.e. the force applied by each individual muscle – can illustrate how muscles co-activate to perform tasks and the role each muscle plays in a complex movement. Since multiple muscles often span a single joint, it is not possible to quantify individual muscle force solely from measurement of joint/limb kinematics and kinetics. Unfortunately, direct measurement of muscle force is infeasible *in vivo* in humans as this typically requires removal of the tissue from its natural space [3], and other indirect approaches suffer from methodological limitations. While recent methods have been proposed for measuring *in vivo* force of specific muscles [4], these methods share the limitations of sEMG in that they are not able to measure contributions of non-superficial muscles that are very important for hand and wrist movements.

Several methods have recently been proposed to estimate individual muscle force using indirect measurements of muscle activity. The primary method used in many studies to quantify muscle activity has been sEMG [3], [5]. This technique has been used effectively in multiple studies analyzing muscle activation in both static [6] and dynamic [7]–[9] contraction, muscle recruitment [10], and limb kinematic data [11]. However, in cases where non-superficial muscles contribute significantly to joint torque production, such as it is in the case of the forearm muscles controlling hand and wrist motion responsible for object manipulation. sEMG-based estimates of muscle forces can be substantially inaccurate [10].

Another technique for analyzing the activation of individual muscles is shear wave elastography (SWE), an ultrasound technique that uses a high-intensity pulse to produce shear waves that propagate through the tissue, and which can be imaged with the ultrasound device [12]. Previous applications of SWE include analysis of activation of both muscles and tendons in healthy [13] and pathologically affected states, including stroke [14] and cerebral palsy [15]. While SWE can provide reasonable estimates of muscular activation for both surface and deep muscles non-invasively, the limited field of view (FOV) provided by ultrasound techniques does not allow for the simultaneous estimation of the mechanical properties of

---

Department of Biomedical Engineering, University of Delaware, Newark DE, 19713. AZ is affiliated with Haexel Robotics, Rome Italy, 00142. MDJM is affiliated with the Thayer School of Engineering, Dartmouth College, Hanover, NH, 03755. * Correspondence e-mail: CLJ: clj@udel.edu; FS: fabs@udel.edu
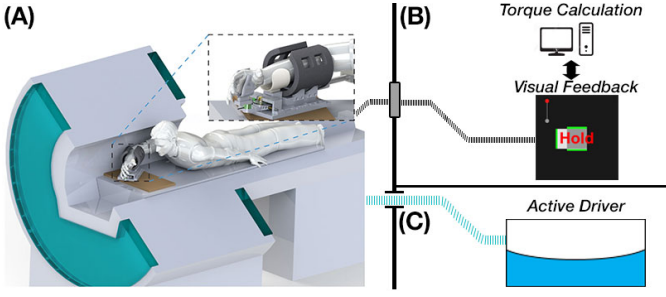
Fig. 1. Setup for multi-muscle magnetic resonance elastography. (A) Subjects are positioned headfirst and prone with their right arm placed in a custom MRE driver and perform isometric contractions cued by (B) the visual feedback system that allows the subject to visualize and maintain applied torque. (C) The MRE driver is connected to a pneumatic actuator.

a large number of muscles during a single contraction [16], as are used in tasks involving the hand and wrist. Therefore, any variation in activation between data collections will provide an inaccurate estimation of the total tissue response.

As a technique similar to SWE, magnetic resonance elastography (MRE) is a magnetic resonance imaging (MRI) technique for non-invasively imaging tissue mechanical properties [17], [18]. MRE uses propagating shear waves from a mechanical actuator – e.g. piezoelectric [19] or pneumatic [20] – to quantify the viscoelastic properties of soft tissues, including the liver and brain. Preliminary skeletal muscle MRE studies demonstrated the relationship between apparent material stiffness and contractile state of the muscle [21]. A recent study by Schrank, et al. [22] used MRE to quantify individual muscle response to activation in real-time and found responses in shear wave velocities with contraction. Similarly, muscle mechanics were investigated with MRE by Debernard, et al. [23] to quantify the age-related changes in muscle stiffness at rest and during contraction in children and middle-aged adults, providing a reference for future analysis of diseased tissue. However, previous uses of MRE in skeletal muscle studies did not simultaneously measure the mechanical properties of the entire set of muscles surrounding a human joint, nor did they quantify an association between the measured mechanical properties and muscle force. As such, it is currently unclear if MRE can be used to quantify muscle coordination strategies employed by humans for interacting with the environment.

In this study, we use MRE to simultaneously measure the shear wave speed in each of the forearm muscles during isometric contractions of the wrist, a technique that we name multi-muscle magnetic resonance elastography (MM-MRE). The primary objective of this study is to determine the sensitivity of MM-MRE to muscle activation and illustrate its effectiveness in simultaneously estimating the force output of multiple muscles active during isometric contractions. We used MM-MRE to quantify stiffness of the individual muscles of the forearm at different levels of muscle activation and at different contraction states, including multiple amplitudes of wrist torque in both flexion and extension and in different wrist postures. We then combined all MM-MRE measurements in a model-based estimation framework to estimate force output from each individual muscle at each contraction state.

II. METHODS

A. Muscle Mechanics

Outcomes from MRE typically include the complex shear modulus, $G*$, from which we can consider the shear stiffness, or the square of the shear wave speed or velocity. In order to quantify muscle-specific forces from measurements of shear wave velocity, we need to note some preliminary considerations about (1) the relationship between muscle force and muscle stiffness, (2) the relationship between shear modulus and Young's modulus, and (3) the relationship between the shear wave velocity and the load and stiffness of the muscle. First, muscle force (f_{MT}) is related to the axial stress (σ) through the muscle's cross-sectional area (A_{CS}):

$$\sigma = \frac{f_{MT}}{A_{CS}} \tag{1}$$

The short-range stiffness model is a widely accepted model that describes the stiffness properties of skeletal muscle during isometric contractions to be dependent on the force produced by that muscle [24], [25]. Short-range stiffness is derived from the cross-bridge muscle model and suggests that an increase in the actin-myosin cross-bridges results in an increase in the muscle axial stress and stiffness. In the short-range stiffness model, under isometric contractions, it is assumed that the Young's modulus, E, increases linearly with axial stress (σ) with slope α, from an unstressed value E_0:

$$E = \alpha\sigma + E_0 \tag{2}$$

While a linear relationship between Young's modulus and shear modulus is only valid for isotropic and homogeneous materials, Eby et al. [13], showed a linear relationship between Young's modulus, E, and shear modulus, G, for skeletal muscle, even though skeletal muscles are anisotropic materials. With this approximation, we can quantify the stiffness of the muscle based on measurements of shear modulus, provided that the slope β of such a linear relationship is known.

$$G = \frac{E}{\beta} \tag{3}$$

In axially isotropic tissues, such as tendon and muscle fibers, shear wave velocity is a function of both shear modulus and axial load. Martin, et al. [4] showed that shear wave velocity, $v_{SH,}$ in tendons and muscle fibers can be described by the model of a tensioned Timoshenko beam:

$$v_{SH}^2 = \frac{k'G + \sigma}{\rho} \tag{4}$$

where ρ is the density of the material and k' is a shear correction factor ranging from 0 to 1. Given these premises and substituting Eqn. (2) and (3) in Eqn. (4), it is possible to describe the relationship between shear wave velocity and axial load:

$$v_{SH}^2 = \frac{\frac{k'\alpha}{\beta} + 1}{\rho}\sigma + \frac{k'E_0}{\beta\rho} \tag{5}$$

Thus, by substituting Eqn. (1) into Eqn. (5) we can describe a relationship between shear wave velocity and muscle force:

$$v_{SH}^2 = \frac{\frac{k'\alpha}{\beta} + 1}{\rho A_{CS}}f_{MT} + \frac{k'E_0}{\rho\beta} = \gamma^{-1}f_{MT} + C \tag{6}$$

In this expression, $\gamma = \frac{\rho A_{CS}\beta}{k'\alpha + \beta}$ and $C = \frac{k'E_0}{\rho\beta}$ are muscle-specific constants accounting for the linear relationship

between shear wave speed squared and force. This relationship can be inverted to calculate muscle force given measurements of shear wave speed as:

$$f_{MT} = v_{SH}^2 \gamma - k \qquad (7)$$

All considered, individual muscle force can be estimated from measurements of shear wave velocity once having determined the set of muscle-specific proportionality constants γ and k.

B. Experimental methods

We collected data on human participants using a Siemens 3T Prisma MRI scanner (Siemens Healthineers; Erlangen, Germany). Participants were positioned headfirst and prone, as seen in Fig. 1A, with their right arm forward in a custom-built actuation device. This device incorporated a passive driver for delivering vibrations to the tissue through the muscle belly of the forearm and was connected to the Resoundant active pneumatic actuator (Rochester, MN) in the MRI control room, Fig. 1C. Additionally, the device held the flexible MRI coil that wrapped around the forearm and had a pair of supports and restraints for the hand and wrist. The participant's forearm rested on the passive driver, approximately below the ulna, and the flexible coil was gently wrapped around the arm to apply minimal pre-compression to the tissue. The participant's hand and wrist were constrained by an MRI-compatible robotic device, referred to as the MREbot [26]. A force/torque sensor (Mini27Ti, ATI Industrial Automation, Apex, NC) was connected to the base of the hand support to which force was applied by the participant, with visual feedback, as seen in Fig. 1B, provided to cue the proper application of joint torque during scanning through a VisuaStimDigital (Resonance Technology) audio-visual system. Additional details on the setup and device are provided in our previous publication [26].

We scanned thirteen healthy, young adult participants (11/2 M/F; age range: 22-35 years, BMI range: 21.5-27.4 kg/m^2) through the wrist activation protocol. The study was approved by the Institutional Review Board of the University of Delaware (IRBNet ID: 1465242-5) and each participant provided written informed consent before participation. The inclusion criteria of the study included no history of central nervous system disease or brain injury, no condition affecting bones, tendons, ligaments, or muscles in the arm, no acute or chronic back pain, non-pregnant, and no conditions compromising safety in the MRI. The protocol consisted of 45 MRE scans divided between three wrist postures as defined by the angle about the flexion/extension (FE) axis, $\theta_{FE} = [-15, 0, 15]°$. A positive angle indicates a flexed wrist, a negative angle indicates an extended wrist, and zero indicates a neutral position. The wrist was held in a neutral angle about the radial/ulnar direction (RUD) axis. To achieve these wrist postures, subjects manually adjusted the device by unlocking from one posture and then adjusting the wrist angle and relocking the hand support into the new posture. The order of wrist posture was neutral, extended, then flexed for all subjects. At each wrist posture, 15 MRE scans were collected with three scans at each of the five activation states, defined by joint torque values $[\tau_{FE}; \tau_{RUD}] = [\{-1; 0\}, \{-0.5; 0\}, \{0; 0\}, \{0.5; 0\}, \{1; 0\}]$ N·m. Thus, torque was applied in both wrist flexion and extension, at two

magnitudes, but no torque was applied about the axis of radial/ulnar deviation. Also, MRE data were collected in a rest condition. The order of the 15 scans performed in each wrist posture was randomized for each subject. During each of these scans, the subjects were cued to apply and hold the designated contraction condition for the entire duration of the scan (i.e., 21 s) through the visual feedback system. The subject was given time to relax during each of the anatomical scans for each posture.

We used an echo-planar imaging MRE sequence with the following parameters: 2 x 2 x 3 mm^3 voxel size; FOV = 128 x 128 mm^2; 15 slices; TR/TE = 1314/41 ms; vibration frequency = 80 Hz; 4 phase offsets; single gradient polarity; time = 21 seconds per MRE scan. Complex-valued displacement amplitudes at the vibration frequency were computed by Fourier transform across the 4 phase offsets. For each posture, an anatomical scan was also performed after the MRE scans to allow for region-of-interest (ROI) identification. The anatomical scan was a T$_2$-weighted BLADE (motion insensitive, multi-shot, turbo spin echo) sequence, acquired with the following parameters: 1 x 1 x 3 mm^3 voxel size; FOV = 128 x 128 mm^2; slices = 60; TR/TE = 9520/79 ms. Each T$_2$-weighted anatomical scan required 210 s of acquisition time. The total scan time per subject was approximately 35 minutes.

C. MRE image analysis

Muscle tissue, like other biological tissues, is known to exhibit viscoelastic behavior, with both energy storage (elastic) and loss (viscous) characteristics [27], [28], and both parameters affect the propagation of shear waves in the tissue. We used the imaged displacement fields from MRE (Fig. 2B) to estimate the shear wave speed through the viscoelastic muscle tissue of the forearm using the nonlinear inversion algorithm (NLI) [29]. NLI determines tissue mechanical properties using a finite element-based inverse problem solved by iteratively minimizing the objective function:

$$\Phi(\theta) = \sum_{i=1}^{N_m} \left\{ \left(u_{m(i)} - u_{c(i)}(\theta) \right) \left(u_{m(i)} - u_{c(i)}(\theta) \right)^* \right\} (8)$$

where $u_{m(i)}$ represents the complex-valued amplitude of the ith displacement measurement location, $u_{c(i)}(\theta)$ is the analogous displacement computed from a finite element model using current estimate of the properties, θ, N_m is the number of measurements and * represents the complex conjugate [27]. NLI models the material as a heterogeneous, isotropic, linear viscoelastic material which is governed by Navier's equation,

$$\nabla \cdot \left(G^*(\nabla \vec{u} + \nabla \vec{u}^T) \right) + \nabla(\lambda \nabla \vec{u}) = -\rho \omega^2 \qquad (9)$$

where $\vec{u}$ is the 3D displacement field, λ is the first Lamé material parameter and G^* is the second, or the shear modulus, ω is the speed of the propagating shear wave, and ρ is the density (assumed to be 1000 kg/m^3).

NLI is typically used to estimate material properties of tissue from MRE data to provide metrics of structural integrity. The current NLI implementation uses a linear model, therefore, does not include higher order effects of static prestrain (such as from muscle activation), and returns maps of the apparent complex shear modulus, $G^*| = G' + iG''$, from which we commonly calculate the shear "stiffness", $\mu = 2|G^*||^2/(G' + |G^*||)$. This
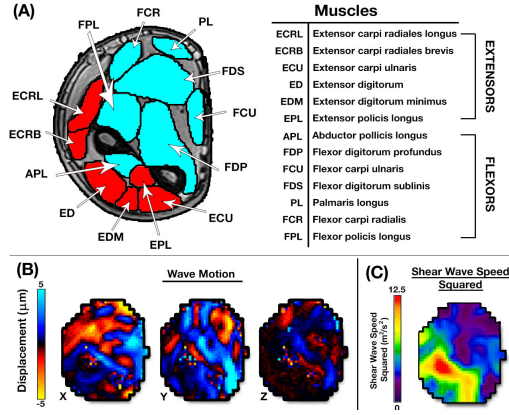
Fig. 2. (A) Each muscle of the thirteen muscles that are involved in wrist motion and analyzed in this study are manually segmented. A representative cross section with a region of interest defining each of the muscles is shown. (B) Shear wave motion generated throughout the forearm from actuation at 80 Hz and captured in 3D by the MRE sequence. (C) Map of shear wave speed squared estimated from wave motion by the nonlinear inversion algorithm (NLI).

parameter is itself related to the wave speed through a viscoelastic material [17]. In this application, we are primarily interested in wave speed, as this has been shown to change with loading of muscle tissue [30], [31], thus we report the shear wave speed squared (SWSS) as $v_{SH}^2 = \mu/\rho$.

We determined the SWSS in each condition in thirteen individual muscles of the forearm. Muscles were manually segmented to generate individual ROI masks using the T_2-weighted anatomical images as a reference. The muscle regions were then registered to MRE image space using FMRIB's Linear Registration Tool (FLIRT) from FMRIB's Software Library (FSL) [32] to create binary masks for analysis. The 13 muscles segmented for analysis are: abductorpollicis longus (APL), extensor pollicis longus (EPL), extensor digitorum (ED), extensor digitorum minimus (EDM), extensor carpi radialis longus (ECRL), extensor carpi radialis brevis (ECRB), flexor carpi radialis (FCR), palmaris longus (PL), flexor digitorum sublimis (FDS), flexor carpi ulnaris (FCU), flexor digitorum profundus (FDP), and flexor pollicis longus (FPL), as shown in Fig. 2A.

To investigate the response of MM-MRE wave speed outcomes to active muscle tension, we compared the estimated SWSS in individual muscles due to several factors: muscle type; activation state; and wrist posture. Additionally, these factors are compared at both the muscle group level and individual muscle level. Statistical analysis consisted of a linear mixed model, with fixed effects of muscle type, activation state, and wrist posture and the interactions of each of these factors. Participant and muscle were included as random effects (repeated measures factor), along with the interaction of muscle with the fixed effects of muscle type, activation state, and wrist posture. Factor "muscle" was used as a nested factor within factor "muscle type" to allow grouping of measured effects between muscles with a supposedly similar activation pattern across the other two fixed factors. Due to the complexity of the model output, post-hoc Tukey tests were conducted on model-estimated coefficients for the muscle group and muscle-specific analysis for visualization purposes. Post-hoc Tukey tests were performed to determine the effect of agonist and antagonist

contraction on SWSS for all muscles. Then, post-hoc Tukey tests were performed to compare SWSS at each of the different activation states for the extensors and flexors, separately. Post-hoc Tukey tests were performed to compare the effect of activation state for both the extensors and flexors at each different wrist posture, separately. Finally, post-hoc Tukey tests were performed on the individual muscle level at each of the wrist postures to test for different levels of SWSS between torque application levels. For muscle specific analyses, Cohen's D effect sizes, defined as the ratio between the mean between-subjects change in SWSS relative to rest (for each muscle, posture, and contraction level) and the standard deviation of this change, were reported for each relationship between active contractions and their corresponding resting condition. Following post-hoc tests, all averaged SWSS values for each activation state were normalized by dividing the averaged SWSS value during the rest condition used in the post-hoc comparison.

D. MRE-based force estimation

To determine the set of muscle-specific γ and k values, we utilized a forward dynamics muscle force estimation procedure extending the one presented in previous work [33]. The muscle force estimator combines measurements of SWSS, wrist torques, and wrist postures with parameters extracted from a musculoskeletal model [34]. No subject-specific modifications or scalings were done. The musculoskeletal model includes thirteen muscles spanning the fingers, wrist, and elbow joints. A muscular Jacobian matrix, J, was obtained for each of the 13 muscles and wrist postures from the musculoskeletal model via OpenSim [34]. The same muscular Jacobian matrix was used for all subjects. Components of matrix J are the moment arm values with each row corresponding to a wrist DOF, FE or RUD, and each column corresponding to a specific muscle, resulting in J being a 2×13 matrix. Therefore, all contractions at a single posture involved the same muscular Jacobian matrix. For estimation, a 2×1 wrist torque vector ($\boldsymbol{\tau} = [\tau_{FE}; \tau_{RUD}]$) measured during each isometric contraction is related to the 13 $\times$ 1 muscle force vector through the equation below:

$$\boldsymbol{\tau} = -J f_{MT} \tag{10}$$

Through substituting the relationship between muscle force and shear wave speed into the previous equation, we obtained the relationship between the measurements of SWSS and the wrist torques:

$$\boldsymbol{\tau} = -J\Gamma v_{SH}^2 + Jk \tag{11}$$

where v_{SH}^2 is a 13×1 vector that contains the measurements of SWSS for each muscle, $\boldsymbol{\Gamma} = \text{diag}(\gamma_1, \gamma_2, ..., \gamma_{13})$ is a 13×13 matrix that contains muscle-specific slope constants in its diagonal elements, and $\boldsymbol{k}$ is a 13×1 vector that contains the muscle-specific offset constants.

Overall, Eqn. (11) is a linear equation of the form $X_l\boldsymbol{\beta} - \boldsymbol{y} = \mathbf{0}$, where $X_l = [M\ J]$ is a 2×26 matrix obtained by horizontal concatenation of matrices J (Jacobian) and M (a 2×13 matrix with elements $M_{ij} = -J_{ij}v_{SH,j}^2$); $\boldsymbol{\beta} = [\boldsymbol{\gamma}; \boldsymbol{k}]$ is a 26×1 vector of unknowns obtained by vertical concatenation of the unknown parameter vectors $\boldsymbol{\gamma} = (\gamma_1, \gamma_2, ..., \gamma_{13})^T$ and $\boldsymbol{k} = (k_1, k_2, ..., k_{13})^T$ and $\boldsymbol{y} = \boldsymbol{\tau}$, and subscript l indicates each

contraction. By collecting data during N isometric contractions at different wrist postures, it is possible to construct a $2N \times 26$ matrix $X = [X_1; X_2; ...; X_N]$ via vertical concatenation of the contraction-specific X_l matrices. For measurements of SWSS obtained in different postures, the different terms Jv_{SH}^2 in X_l will be linearly independent across contractions, and thus matrix X is guaranteed to be full-rank. Using a least squares regression model, it is then possible to estimate the vectors γ and k given measurements of joint torque, shear wave velocity, and knowledge of the moment arm matrix J from a musculoskeletal model. After estimating γ and k, the estimated parameters can be used to convert measurements of shear wave speed to estimates of muscle force using Eqn. (7).

Under the model assumptions, the force measured from multiple muscles spanning the wrist joint should sum as described in Eqn. (11) to yield the measured value of joint torque. In other words, if $\widehat{\gamma}$ and $\widehat{k}$ are the estimated muscle-specific parameters for each participant, and $\widehat{\Gamma} = \text{diag}(\widehat{\gamma})$ the joint torques resulting from the estimated muscle forces $\tau_e = -J\widehat{\Gamma}v_{SH}^2 + J\widehat{k}$ should be equal to joint torque values τ_m measured via the F/T sensor. For each participant, we used an ordinary least squares regression model based on Eqn. (11) to estimate the parameters $\widehat{\gamma}$ and $\widehat{k}$. Then, as a proxy to quantify the accuracy of muscle force estimation, we quantified the torque estimation error e_τ, separately, for each contraction,

$$e_\tau = \|\tau_m - \tau_e\| \tag{12}$$

Through the linear regression model, we obtained R^2 goodness of fit values for each subject to evaluate how well the SWSS measurements accounted for the variability in wrist torque values. Finally, we quantified the average estimated wrist torque error for all subjects, postures, repetitions at each contraction state to determine the overall torque error associated with a contraction.

III. RESULTS

The results of the linear mixed model performed to assess the effects of muscle type and recruitment, activation state, and wrist posture on measured SWSS at the muscle group level are reported in Table 1. Multiple significant interactions were found at the individual and combined effect levels of interactions, though wrist posture appeared to be the least stable predictor of muscle activation, with the lowest F-value of all individual predictors. Extensors exhibited higher SWSS than flexors. Activation state appeared to be the strongest indicator of SWSS with the highest F value of all the individual factors.

The differences in normalized SWSS was more apparent when comparing the muscles in their agonist and antagonist state for all subjects, wrist postures, repetitions, and muscles, as shown in Fig. 3, where we found significant differences in all important agonist-antagonist comparisons: active vs rest states, low vs high applied torque, and corresponding agonist and antagonist action at both applied torques. The data shows an average increase of 15% and 10% during 1.0 and 0.5 N·m of torque, respectively, when acting as an agonist, and 8% and 3% during 1.0 and 0.5 N·m of torque, respectively, when acting as an antagonist.
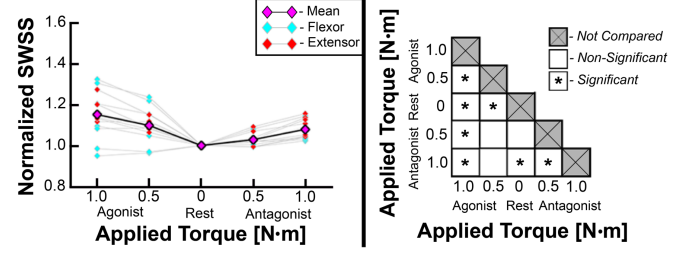

Fig. 3. (Left) Normalized shear wave speed squared speed (SWSS) values for all muscles during agonist and antagonist contractions, at both 0.5 and 1.0 N·m. Averages are connected via black lines while individual muscle data are connected via gray lines. (Right) Map of significant differences between activation states for agonist and antagonist muscles. Statistical significance ($p<0.05$) of post-hoc tests is denoted by *.

Fig. 4 shows the combined average normalized SWSS values across all repetitions, all wrist postures, and all subjects, but separated by whether the muscles are flexors or extensors. Both the flexor and extensor muscles showed significant increases in SWSS during flexion and extension activations, shown in Fig. 4. Flexors showed an increase of 13% and 10% during 1.0 N·m and 0.5 N·m of flexion, respectively, and 6% and 2% during 1.0 N·m and 0.5 N·m of extension, respectively. Extensors showed an increase of 10% and 4% during 1.0 N·m and 0.5 N·m of flexion, respectively, and 17% and 10% during 1.0 N·m and 0.5 N·m of extension, respectively. Shown in Fig. 5 are the effects of altering wrist posture on the flexor and extensor muscle SWSS outcomes across the five activation states. Extensors show significantly greater SWSS during the maximum agonist isometric contraction compared to rest in all postures, while flexors show significantly greater SWSS than rest in all postures except wrist extension (-15°). Both muscle groups engage differently during contractions based upon alterations in wrist posture. While flexors appear to show overall increases in relative SWSS during activation while in the non-neutral wrist postures, the extensors react in an opposite manner, exhibiting decreased relative SWSS in the non-neutral wrist postures,

TABLE I
RESULTS OF THE LINEAR MIXED MODEL ANALYSIS OF SWSS PREDICTORS

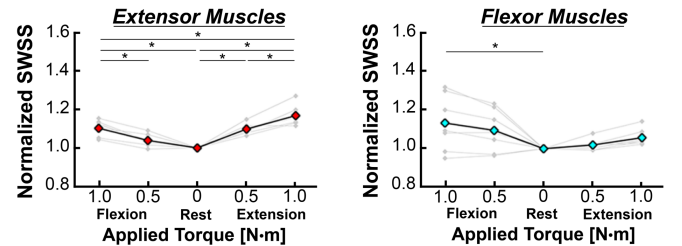| Predictor	DOF	F	p value
Muscle type	1	16.51	**0.0019**
Activation state	4	17.31	**<0.0001**
Wrist posture	2	13.31	**0.0002**
Muscle type × activation state	4	8.84	**<0.0001**
Muscle type × wrist posture	2	5.42	**0.0122**
Activation state × wrist posture	8	8.95	**<0.001**
Muscle type × activation state × wrist posture	8	3.70	**0.0009**

Fig. 4. Normalized SWSS values for the extensor (left) and flexor (right) muscles during each of the contraction states, at both 0.5 and 1.0 N·m. Averages are denoted via colored diamonds and connected via black lines, while individual muscle averages are in light gray. Statistical significance ($p<0.05$) of post-hoc tests is denoted by *.
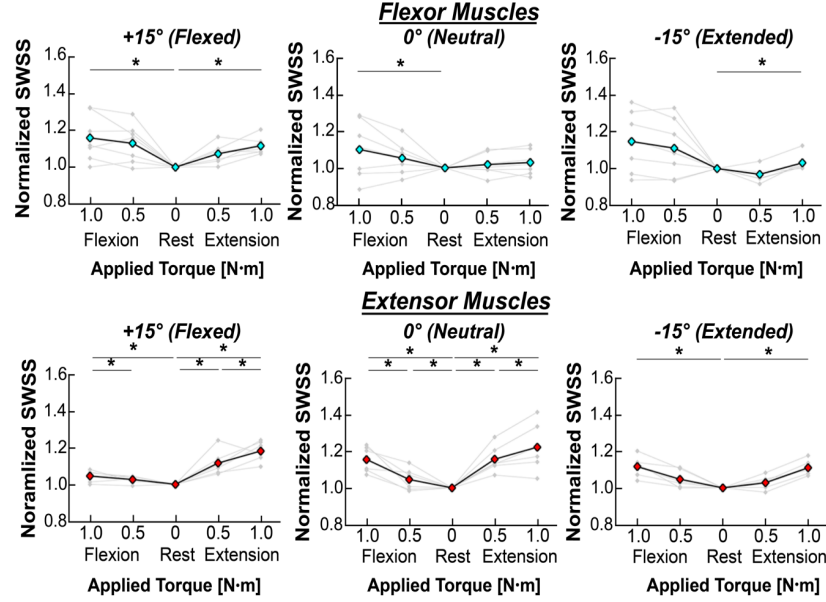
Fig. 5. Normalized SWSS for the flexor (Top) and extensor (Bottom) muscles at different wrist postures. The average of each muscle group is shown in colored diamonds and black lines, while the individual muscle averages are in light gray. Statistical significance ($p<0.05$) of post-hoc tests is denoted by *.

when compared at the same activation state. With the muscle group level variations presented in Fig. 5, we further investigated the effects of altering wrist posture along with activation state at the individual muscle level in Fig. 6.

In Fig. 6, we show the resulting effect sizes of the individual muscle level comparison for those muscles that show significant differences between one of the activation states and the rest condition for each of the three wrist postures. Many of the forearm muscles show changes in effect size and significance in varying torque output during agonist action as the wrist angle changes, as well as occasionally during antagonist action. Most extensor muscles display significant increases in SWSS at the neutral posture, with at least one muscle showing changes at each activation state. The extensors show fewer individual muscle SWSS responses during the non-neutral postures, though most of these significant changes occur at 1.0 N·m of extension. At all postures, more extensors increase in SWSS during extension than in flexion, supporting the group level analysis findings. As for the flexors, they are mostly consistent across the three wrist postures, with muscles showing increases at both 1.0 N·m and 0.5 N·m in flexion, with more increases in SWSS at higher levels of activation and

during the agonist action of flexion.

The range of goodness of fit (R^2) values obtained in back-estimating joint torques was, for the different subjects, 0.69 ± 0.17 with an average torque estimation error of 0.32 N·m ranging between 0.24 N·m (Rest condition) and 0.43 N·m (1 N·m Flexion condition). The estimation error was highly dependent on the type of contraction considered, with lower error associated with the 0.5 Nm contractions than with the 1 Nm contraction. Graphical representations of the group level estimated torques are shown in Fig. 7A-B, while the mean and standard deviation of the cross-validation error measured for different contraction states are shown in Fig. 7C. The APL was found to be a data outlier within the model and was excluded during least squares estimation.

IV. DISCUSSION

In this study, we introduced MM-MRE and demonstrated the ability to identify changes to muscular loading by measuring
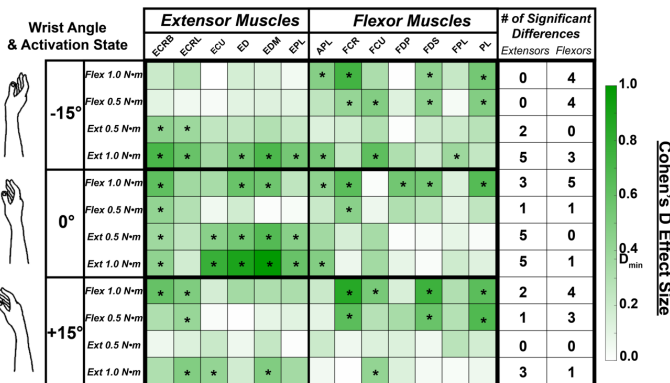

Fig. 6. Cohen's D effect size for statistical differences comparing each activation to the rest condition for each muscle, in each posture. Activations marked with an asterisks (above $D_{min}= 0.37$) are greater than rest at p<0.05.
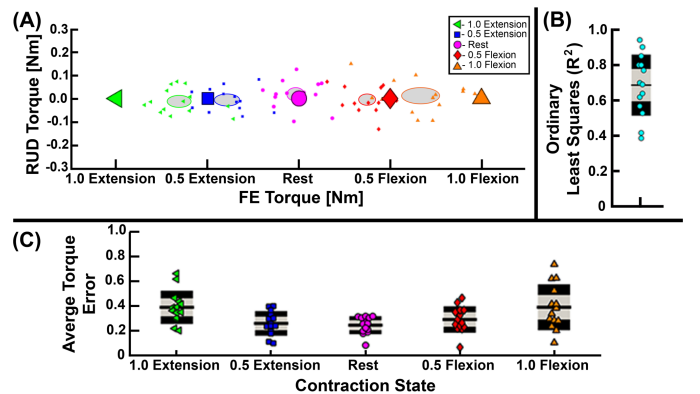

Fig. 7. (A) Estimated torque obtained through muscle force estimation. Average torque estimated across repeats and posture from each participant is reported via a small marker, filled with the color and shape corresponding to the cued contraction state (large markers). The ellipsoids mark the 2D distribution of estimated torque. (B) The average ordinary least squares fit per subject and (C) least squared error per contraction state help provide an overall picture of the models fit.

the shear wave speed in multiple muscles simultaneously, at a variety of activation conditions. Specifically, we compared the effects of agonist vs. antagonist action, activation state, and wrist posture on the shear wave speed measures. Through a musculoskeletal model, we used the measured shear wave speeds to estimate force from individual muscles in performing the wrist tasks. This study demonstrates how MM-MRE can provide insight into the individual and group level responses of muscles during contractile states and study how the muscles in the forearm coordinate to generate isometric force. MM-MRE is a new tool that can be used for elucidating fundamental principles of muscle coordination for tasks involving hand and wrist function, and for quantifying impairment in muscle coordination for hand-wrist muscles in patients affected by neuromotor conditions such as stroke [35]–[37] .

The primary objective of this study was to determine the sensitivity of MM-MRE to muscle activation, specifically by using MM-MRE to measure shear wave speed within the muscles in the forearm under different conditions of muscle activation, conditioned via generation of multiple levels of wrist joint torque. We found significant differences when comparing the activation states with applied torque to the resting states, indicating that increases in the SWSS and apparent stiffness of muscles change with muscular activation and loading, a finding supported by previous MRE [21], [22] and ultrasound elastography research [31], [38]. By taking data points at multiple torque application states, we determined that the SWSS changed significantly with intensity of torque output. We found significantly higher shear wave speeds for applied torque of 1.0 N·m compared to 0.5 N·m, with both being significantly higher than in the rest condition. This change in shear wave speed results primarily from isometric contraction through which the muscle fibers increase tissue loading, but do not alter in length. This increased loading of the tissue is a phenomenon known as "cross-bridging" [39], [40], which describes myosin chains attaching to bonding sites on actin creating cross-bridges between the two proteins, thus increasing the velocity of propagation of shear waves in the tissue.

Muscular co-contraction is when two groups of muscles, on opposite sides of a joint, are simultaneously activated to regulate joint stability [41]. During co-contraction, muscles are classified into one of two roles: agonist or antagonist. Muscles are considered agonists when the muscles are being used as a primary driver of motion and force application in a direction, and they are considered antagonists when the muscles are being recruited to support and stabilize in response to the agonistic activation. We found significant differences in how the muscles responded by comparing how the flexor and extensor muscles acted in their agonist and antagonist states. Both flexors and extensors showed significant increases in shear wave speed during both agonistic and antagonistic action compared to the rest condition, indicating that both are being recruited as a part of co-contraction and that MM-MRE is sensitive to such activation. We also found that all forearm muscles showed significantly higher shear wave speed when being recruited for their agonist action as the primary force output compared to when these muscles are acting as antagonists or are in a primarily stabilizing role, as expected.

Researchers studying muscular co-contraction with other methods including sEMG and SWE have found similar results to those found in this study, though with key differences. For instance, Raiteri, et al. [38] used SWE along with sEMG to quantify agonistic and antagonistic responses of the lateral gastrocnemius of the calf and also found a higher shear wave speed during agonist action. However, though the study found increased sEMG outputs during antagonist activation, they did not detect increased shear wave speed, instead finding negligible changes. Using an MRE technique, Schrank, et al. [22] found overall similar results to the outcomes found in this study with increases in measured shear wave speed in lower leg muscles during both agonist and antagonist conditions, with agonist action resulting in higher wave speed than antagonist.

Another important aspect of measuring these shear wave speed outcomes in skeletal muscles is the level of pre-loading due to initial tension level. Every muscle has a resting level of tension when at a neutral posture, as opposed to being slack or overstretched [42], which can affect whether muscles appear to have significantly higher SWSS during contraction. In this study, we aimed to quantify if and how changes to these tension levels altered the responses of the measured shear wave speed by changing the wrist posture and inducing passive flexion and extension. We subsequently found differences in the response of the forearm muscles both at the muscle group and individual muscle level of response. As shown in this study, we found higher percentage changes in shear wave speed and larger effect sizes when muscles were passively shortened and given slack with the opposite occurring during increased tension levels. We hypothesize this response is due in part to two biological effects: either (A) higher rest condition shear wave speed due to increased passive tension or (B) the muscle length or tension level alters the ability of the muscles to generate the necessary force during isometric contraction.

Previous studies have shown a positive correlation between passive muscle tension and muscle length [38], which agrees with the changes in wrist posture shown in this study. Additionally, recent MRE studies showed a positive relationship between shear wave speed and muscle length during passive flexion and lengthening in the calf [43],[44]. The mechanism for this increase in muscle tension is possibly tied to a third structural protein within sarcomeres known as titin [45], [46]. Multiple studies have shown that titin is a primary cause of passive force enhancement during isometric contraction as it acts as a molecular spring, altering stiffness during muscular activation and maintaining force in muscles that are stretched to long lengths, such as those during changing wrist postures. Another possible cause for this change in muscle tension is the stretching of collagen based structures, such as epi-, peri- and endomysium and muscle fiber extracellular matrices [47].

In addition to the MRE-based component of this study, we presented a muscle force estimation framework that converts measurements of SWSS to individual muscle forces based on the linear relationship between muscle stiffness and force as accepted in the short-range stiffness model of skeletal muscles.

Via the muscle force estimation framework, we were able to establish that the measured changes in shear wave speed were indeed associated with changes in muscle force. With the muscle force estimator validation analysis, some subjects have a strong goodness of fit value, representing a strong linear relationship between shear wave speed squared and wrist torque. This observation provides support for the idea that shear wave speed can be used to accurately estimate muscle force, provided that the geometric model used for describing the change in muscle moment arms in the different postures is correct. However, estimates from a small number of subjects have a weak goodness of fit to experimental data. Thus, there is a need to further investigate the muscle force estimation with experimental data before its accuracy can be validated. When grouping measurements from all individuals, the estimated torque error ranges from 40% to 80% which is substantially high error. This limitation may be due to the fact that the selected experimental design only included isometric torque contractions only in the flexion/extension direction, while the muscle force estimator was developed to use measurements resulting from contractions in both the flexion/extension and radial/ulnar deviation direction [33]. The high error may also come from limitations in the model used to estimate force or the assumption of a linear relationship between force and observed SWSS. Future directions include employing MM-MRE in a two-degree-of-freedom design with isometric wrist contractions applied in both the flexion/extension and radial/ulnar deviation directions and from this new experiment we expect to improve the goodness of fit values and reduce the torque estimation error associated with muscle force estimates.

V. LIMITATIONS

The current version of this technique has limitations associated with the signal-to-noise ratio achievable within a given amount of time, while imaging with sufficient resolution to capture individual wrist muscles [48], [49]. Muscle contraction presents a unique problem within the realm of MRE as it limits the possible acquisition time of each scan before muscle fatigue sets in from excessive loading, particularly at larger loads [45]. Once muscle fatigue occurs, the data is prone to additional noise and artifacts from subject motion. To account for this, the scanning time is shortened to acquire the best data possible in the limited time frame.

Another data quality challenge of MM-MRE is the inclusion of the bones within the acquired volume and the size of the bones compared to the forearm muscles. Forearm muscles are relatively small when compared to those in other appendages and though the bones are also smaller, their size relative to the muscles is larger. The material model used in NLI does not apply to bone as bone is several orders of magnitude stiffer than the surrounding tissues of interest, thus causing data-model mismatch and uncertainty in the outcomes. An effect of this data quality challenge was the removal of the APL during the modeling process. The APL primarily resides within the gap between the ulna and radius and mostly sits, as seen in Fig. 2A, with the extensor muscles, even though its agonist motion is

flexion. Due to these two issues, SWSS results in the APL were heavily affected by noise and were also significantly different than other flexor muscles, prompting APL removal from modeling.

Using isotropic models for skeletal muscle will suffer some bias as apparent stiffness changes due to muscle forces are expected primarily along the muscle axis, whereas the isotropic stiffness estimates are an average of stiffness in each direction (weighted by the proportion of wave energy propagating in each direction) [50], [51]. Recent studies have utilized mechanically anisotropic material models for parameter estimation because of the fibrous nature of the tissue and directionally applied stresses [43], [44], [52]–[54]. In this study we used an isotropic MRE approach due the imaging time requirement for anisotropic MRE including diffusion MRI data in addition to MRE with at least two different displacement fields at each condition [55]. Future studies of the forearm MRE problem using anisotropic techniques may produce more accurate force estimates by capturing stiffness changes in each direction independently.

VI. CONCLUSION

In this study, we quantify the sensitivity of MM-MRE to the activation of skeletal muscles in the forearm by collecting MRE data during a variety of contraction conditions and wrist postures. The MM-MRE outcomes of SWSS are then used with a muscular model to estimate the individual contributions of each of the forearm muscles. MM-MRE showed increases of SWSS during varying levels of contraction and signs of co-contraction activation with agonist and antagonist activity, including significant differences between how a muscle reacts when being recruited into one of these two functions. Furthermore, we discovered how changing the posture of the wrist, and therefore the length of the muscles, affected the different muscle activations. We showed promising results while using the SWSS estimations from MM-MRE to estimate the force contributions of the individual muscles. Future directions of this work include application of this technique to quantify motor impairment of individuals with stroke and cerebral palsy.

REFERENCES

[1]   J. R. Flanagan, M. C. Bowman, and R. S. Johansson, "Control strategies in object manipulation tasks," *Current Opinion in Neurobiology*, vol. 16, no. 6, pp. 650–659, Dec. 2006.

[2]   A. Hassan H., "Monitoring of neuromuscular function," pp. 261–78, 1989.

[3]   T. J. Roberts and A. M. Gabaldón, "Interpreting muscle function from EMG: lessons learned from direct measurements of muscle force.," *Integrative and comparative biology*, vol. 48, no. 2, pp. 312–20, Aug. 2008.

[4]   J. A. Martin *et al.*, "Gauging force by tapping tendons," *Nature Communications*, vol. 9, no. 1, pp. 1–9, Apr. 2018.

[5]   K. R. Mills, "The basics of electromyography," *Journal of Neurology, Neurosurgery & Psychiatry*, vol. 76, no. suppl 2, pp. ii32–ii35, Jun. 2005.

[6]   N. Nazmi, M. A. A. Rahman, S. I. Yamamoto, S. A. Ahmad, H. Zamzuri, and S. A. Mazlan, "A Review of Classification Techniques of EMG Signals during Isotonic and Isometric Contractions," *Sensors (Basel, Switzerland)*, vol. 16, no. 8, Aug. 2016.

[7]   T. S. Buchanan, D. G. Lloyd, K. Manal, and T. F. Besier,

"Neuromusculoskeletal modeling: estimation of muscle forces and joint moments and movements from measurements of neural command.," *Journal of applied biomechanics*, vol. 20, no. 4, pp. 367–95, Nov. 2004.

[8] D. M. Rouffet and C. A. Hautier, "EMG normalization to study muscle activation in cycling," *Journal of Electromyography and Kinesiology*, vol. 18, no. 5, pp. 866–878, Oct. 2008.

[9] D. E. Geiger, F. Behrendt, and C. Schuster-Amft, "EMG Muscle Activation Pattern of Four Lower Extremity Muscles during Stair Climbing, Motor Imagery, and Robot-Assisted Stepping: A Cross-Sectional Study in Healthy Individuals," *BioMed Research International*, vol. 2019, pp. 1–8, Mar. 2019.

[10] A. V. Dieterich *et al.*, "Spatial variation and inconsistency between estimates of onset of muscle activation from EMG and ultrasound," *Scientific Reports*, vol. 7, no. 1, p. 42011, Feb. 2017.

[11] J. G. Ngeo, T. Tamei, and T. Shibata, "Continuous and simultaneous estimation of finger kinematics using inputs from an EMG-to-muscle activation model," *Journal of NeuroEngineering and Rehabilitation*, vol. 11, no. 1, p. 122, Aug. 2014.

[12] M. S. Taljanovic *et al.*, "Shear-Wave Elastography: Basic Physics and MusculoskeletalApplications," *Radiographics*, vol. 37, no. 3, p. 855, 2017.

[13] S. F. Eby, P. Song, S. Chen, Q. Chen, J. F. Greenleaf, and K. N. An, "Validation of shear wave elastography in skeletal muscle," *Journal of Biomechanics*, vol. 46, no. 14, pp. 2381–7, 2013.

[14] S. Eby *et al.*, "Quantitative Evaluation of Passive Muscle Stiffness in Chronic Stroke," *American journal of physical medicine & rehabilitation*, vol. 95, no. 12, p. 899, Dec. 2016.

[15] J. E. Brandenburg *et al.*, "Quantifying passive muscle stiffness in children with and without cerebral palsy using ultrasound shear wave elastography.," *Developmental medicine and child neurology*, vol. 58, no. 12, pp. 1288–1294, Dec. 2016.

[16] S. F. Bensamoun *et al.*, "Determination of thigh muscle stiffness using magnetic resonance elastography," *Journal of Magnetic Resonance Imaging*, vol. 23, no. 2, pp. 242–247, Feb. 2006.

[17] A. Manduca *et al.*, "Magnetic resonance elastography: Non-invasive mapping of tissue elasticity," *Medical Image Analysis*, vol. 5, no. 4, pp. 237–254, Dec. 2001.

[18] L. V Hiscox *et al.*, "Magnetic resonance elastography (MRE) of the human brain: technique, findings and clinical applications," *Physics in Medicine and Biology*, vol. 61, no. 24, pp. R401–R437, Dec. 2016.

[19] I. Sack, B. Beierbach, U. Hamhaber, D. Klatt, and J. Braun, "Non-invasive measurement of brain viscoelasticity using magnetic resonance elastography," *NMR in Biomedicine*, vol. 21, no. 3, pp. 265–271, Apr. 2008.

[20] C. L. Johnson *et al.*, "Local mechanical properties of white matter structures in the human brain," *NeuroImage*, 2013.

[21] M. A. Dresner, G. H. Rose, P. J. Rossman, R. Muthupillai, A. Manduca, and R. L. Ehman, "Magnetic Resonance Elastography of Skeletal Muscle," *Journal of Magnetic Resonance Imaging*, vol. 13, no. 2, pp. 269–276, 2001.

[22] F. Schrank *et al.*, "Real-time MR elastography for viscoelasticity quantification in skeletal muscle during dynamic exercises," *Magnetic Resonance in Medicine*, vol. 84, no. 1, pp. 103–114, Jul. 2020.

[23] L. Debernard, L. Robert, F. Charleux, and S. F. Bensamoun, "Characterization of muscle architecture in children and adults using magnetic resonance elastography and ultrasound techniques," *Journal of biomechanics*, vol. 44, no. 3, pp. 397–401, Feb. 2011.

[24] P. M. H. Rack and D. R. Westbury, "The short range stiffness of active mammalian muscle and its effect on mechanical properties," *Journal of Physiology*, vol. 240, no. 2, pp. 331–350, 1974.

[25] L. Cui, E. J. Perreault, H. Maas, and T. G. Sandercock, "Modeling short-range stiffness of feline lower hindlimb muscles," *Journal of Biomechanics*, vol. 41, no. 9, pp. 1945–1952, Jan. 2008.

[26] A. Zonnino, D. R. Smith, P. L. Delgorio, C. L. Johnson, and F. Sergi, "MM-MRE: A new technique to quantify individual muscle forces during isometric tasks of the wrist using MR elastography," *IEEE International Conference on Rehabilitation Robotics*, vol. 2019-June, pp. 270–275, Jun. 2019.

[27] M. Van Loocke, C. K. Simms, and C. G. Lyons, "Viscoelastic properties of passive skeletal muscle in compression-Cyclic behaviour," *Journal of Biomechanics*, vol. 42, no. 8, pp. 1038–1048, 2009.

[28] I. Sack, K. Jöhrens, J. Würfel, and J. Braun, "Structure-sensitive elastography: on the viscoelastic powerlaw behavior of in vivo human tissue in health and disease," *Soft Matter*, vol. 9, no. 24, p. 5672, 2013.

[29] M. D. J. McGarry *et al.*, "Multiresolution MR elastography using nonlinear inversion," *Medical Physics*, vol. 39, no. 10, pp. 6388–6396, 2012.

[30] L. A. Chernak, R. J. DeWall, K. S. Lee, and D. G. Thelen, "Length and activation dependent variations in muscle shear wave speed," *Physiological Measurement*, vol. 34, no. 6, pp. 713–721, Jun. 2013.

[31] M. Bernabei, S. S. M. lee, E. J. Perreault, and T. G. Sandercock, "Shear wave velocity is sensitive to changes in muscle stiffness that occur independently from changes in force," *Journal of Applied Physiology*, Sep. 2019.

[32] M. Jenkinson, C. F. Beckmann, T. E. J. Behrens, M. W. Woolrich, and S. M. Smith, "FSL," *NeuroImage*, vol. 62, no. 2, pp. 782–790, 2012.

[33] A. Zonnino and F. Sergi, "Model-Based Estimation of Individual Muscle Force Based on Measurements of Muscle Activity in Forearm Muscles During Isometric Tasks," *IEEE Transactions on Biomedical Engineering*, vol. 67, no. 1, pp. 134–145, Jan. 2020.

[34] K. R. Saul *et al.*, "Benchmarking of dynamic simulation predictions in two software platforms using an upper limb musculoskeletal model," *http://dx.doi.org/10.1080/10255842.2014.916698*, vol. 18, no. 13, pp. 1445–1458, Oct. 2015.

[35] T. E. Twitchell, "The restoration of motor function following hemiplegia in man," *Brain*, vol. 74, no. 4, pp. 443–480, 1951.

[36] J. P. A. Dewald, P. S. Pope, J. D. Given, T. S. Buchanan, and W. Z. Rymer, "Abnormal muscle coactivation patterns during isometric torque generation at the elbow and shoulder in hemiparetic subjects," *Brain*, vol. 118, no. 2, pp. 495–510, 1995.

[37] S. Li, "Spasticity, motor recovery, and neural plasticity after stroke," *Frontiers in Neurology*, vol. 8, no. APR. 2017.

[38] B. J. Raiteri, F. Hug, A. G. Cresswell, and G. A. Lichtwark, "Quantification of muscle co-contraction using supersonic shear wave imaging," *Journal of Biomechanics*, vol. 49, no. 3, pp. 493–495, Feb. 2016.

[39] A. F. . Huxley, "Muscle structure and theories of contraction," *Progress in Biophysics and Biophysical Chemistry*, vol. 7, pp. 255–318, 1957.

[40] A. F. Huxley and R. M. Simmons, "Proposed mechanism of force generation in striated muscle.," *Nature*, vol. 233, no. 5321, pp. 533–538, 1971.

[41] S. Hirokawa, M. Solomonow, Z. Luo, Y. Lu, and R. D'Ambrosia, "Muscular co-contraction and control of knee stability," *Journal of Electromyography and Kinesiology*, vol. 1, no. 3, pp. 199–208, Sep. 1991.

[42] J. T. Viitasalo, "Effects of pretension on isometric force production," *International Journal of Sports Medicine*, vol. 3, no. 3, pp. 149–152, Mar. 1982.

[43] Smith, Daniel R., Caban-Rivera, Diego A., Williams, L. Tyler, Van Houten, Elijah E.W., "In-vivo estimation of anisotropic mechanical properties of the gastrocnemius during functional loading with MR elastography," *Physics in Medicine and Biology*, pp. 0–13, 2023.

[44] B. Babaei *et al.*, "Magnetic Resonance Elastography Reconstruction for Anisotropic Tissues," *Medical image analysis*, vol. 74, Dec. 2021.

[45] W. Herzog, K. Powers, K. Johnston, and M. Duvall, "A new paradigm for muscle contraction," *Frontiers in Physiology*, vol. 6, no. MAY, p. 174, 2015.

[46] W. Herzog, M. Duvall, and T. R. Leonard, "Molecular mechanisms of muscle force regulation: A role for titin?," *Exercise and Sport Sciences Reviews*, vol. 40, no. 1, pp. 50–57, Jan. 2012.

[47] C. Stecco, C. Pirri, C. Fede, C. A. Yucesoy, R. De Caro, and A. Stecco, "Fascial or muscle stretching? A narrative review," *Applied Sciences (Switzerland)*, vol. 11, no. 1, pp. 1–11, Jan. 2021.

[48] M. D. J. McGarry, E. E. W. Van Houten, P. R. Perriñez, A. J. Pattison, J. B. Weaver, and K. D. Paulsen, "An Octahedral Shear Strain-Based Measure of SNR for 3D MR Elastography," *Physics in Medicine and Biology*, vol. 56, no. 13, pp. N153–N164, 2011.

[49] C. L. Johnson *et al.*, "3D multislab, multishot acquisition for fast, whole-brain MR elastography with high signal-to-noise efficiency.," *Magnetic Resonance In Medicine*, vol. 71, no. 2, pp. 477–485, 2014.

[50] M. D. J. McGarry *et al.*, "A heterogenous, time harmonic, nearly incompressible transverse isotropic finite element brain simulation platform for MR elastography," *Physics in Medicine and Biology*, vol. 66, no. 5, p. 055029, 2021.

[51] J. L. Schmidt *et al.*, "Measurement of anisotropic mechanical properties in porcine brain white matter ex vivo using magnetic resonance elastography," *Journal of the Mechanical Behavior of Biomedical Materials*, vol. 79, no. December 2017, pp. 30–37, 2017.

[52] M. A. Green, G. Geng, E. C. Qin, R. Sinkus, S. C. Gandevia, and L. E. Bilston, "Measuring anisotropic muscle stiffness properties using elastography.," *NMR in Biomedicine*, vol. 26, no. 11, pp. 1387–1394, 2013.

[53] J. Guo, S. Hirsch, M. Scheel, J. Braun, and I. Sack, "Three-parameter shear wave inversion in MR elastography of incompressible transverse isotropic media: Application to in vivo lower leg muscles," *Magnetic Resonance in Medicine*, vol. 75, no. 4, pp. 1537–1545, Apr. 2016.

[54] M. McGarry *et al.*, "Mapping heterogenous anisotropic tissue mechanical properties with transverse isotropic nonlinear inversion MR elastography," *Medical Image Analysis*, vol. 78, p. 102432, 2022.

[55] D. R. Smith *et al.*, "Anisotropic mechanical properties in the healthy human brain estimated with multi-excitation transversely isotropic MR elastography," *Brain Multiphysics*, 2022.